Assessing the anisotropic features of spatial impulse responses

Benoit Alary, Pierre Massé, Vesa Välimäki, Markus Noisternig

ASSESSING THE ANISOTROPIC FEATURES OF SPATIAL IMPULSE RESPONSES

Benoit Alary
Acoustics Lab
Dept. of Signal Processing and Acoustics
Aalto University
Espoo, Finland
Benoit.Alary@aalto.fi

Pierre Massé
UMR STMS
Ircam-CNRS-Sorbonne Université
Paris, France

Vesa Välimäki
Acoustics Lab
Dept. of Signal Processing and Acoustics
Aalto University
Espoo, Finland

Markus Noisternig
UMR STMS
Ircam-CNRS-Sorbonne Université
Paris, France

ABSTRACT

The direction-dependent characteristics of late reverberation have long been assumed to be perceptually isotropic, meaning that the energy of the decay should be perceived equal from every direction. This assumption has been carried into the way reverberation has been approached for spatial sound reproduction. Now that new methods exist to capture the sound field, we need to revisit the way we analyze and render the decaying sound field and more specifically, establish the perceptual threshold of direction-dependent characteristics of late reverberation. Towards this goal, this paper proposes the Energy Decay Deviation (EDD) as an objective measure of the directional decay. Based on the deviation of direction-dependent Energy Decay Curves (EDC) to a mean EDC, the EDD aims to highlight the direction-dependent features characterizing the decay. This paper presents the design considerations of the EDD, discusses its limitations, and shows practical examples of its use.

1. INTRODUCTION

Early in the development of artificial reverberators, it was presumed that no audible direction-dependent characteristics were present in the late reverberant sound field due to our inability to distinguish singular reflections within the decay [1, 2]. When introducing the first digital reverberation algorithm [3], Schroeder suggested that the main requirement for a multichannel reverberator was to produce low correlated signals on multiple loudspeakers. The same assumption was carried on as more sophisticated delay networks where introduced to formalize multichannel reverberation [4, 5]. Contributing to this assumption, a common descriptor of the reverberation is the mixing time (t_{mix}), which is described as the moment where the energy is statistically equal in all regions of a space [6, 7]. Although the exact mathematical definition varies throughout the literature [8], it implies that the energy is expected to remain isotropic once the t_{mix} has been reached.

Reproduction techniques such as Directional Audio Coding (DIRAC) [9] aim to enhance the reproduction of ambisonics recordings through time-frequency analysis by identifying the incident directions of non-diffused sound sources and ensuring they are reproduced with high coherence over a smaller area, while keeping the reverberant part spatially diffused and incoherent. As with previous methods, the key assumption is that the reverberant fields can be reduced to a decorrelated and isotropic signal, usually described as diffused in spatial sound reproduction. Diffuseness is a criteria that describes the spatial correlation in a sound field and was first introduced to assess the required characteristics of reverberant chambers [10] and as such, wasn't originally tied to a reproduction method. Similarly to the mixing time, the formal mathematical definition of the diffusion varies through the literature [10–15]. Nonetheless, once a certain diffusion threshold has been met, the reverberant sound field is here again considered isotropic.

Convolution with a spatial impulse response (SIR) encoded in Ambisonics will naturally preserve direction-dependent decay characteristics as long as the spatial resolution is sufficient enough to prevent high coherence between output signals on the target reproduction system. However, the convolutions required for large loudspeaker array can have prohibitive computational costs in some applications. Sound reproduction methods such as the Spatial Impulse Response Rendering (SIRR) [16] and the Spatial Decomposition Method (SDM) [17] have been used to simplify the reproduction of SIRs and have been shown to perform well in perceived sound quality evaluation. Using the signals from a microphone array, these methods identify the most prominent incident direction(s) of energy within a given short time window, as well as within a frequency band in the case of SIRR. As such, these techniques make no direct assumption on the isotropy of the sound field. However, due to the increased density of echos during the later part of an impulse response, the analysis win-

doi:10.25836/sasp.2019.32

dow may not hold the sufficient resolution for the reproduction of a complex anisotropic decay, meaning they are more suited for isotropic decays. While most multichannel artificial reverberation algorithms do not naturally extend to render direction-dependent decay characteristics, recent work [18] introduced the design principles to build a Directional Feedback Delay Network capable of reproducing anisotropic decay. However, more work remains to analyze the output of such reverberators.

Recent studies have shown our capacity to detect small directional energy variations within the decay of noise signals, suggesting the need for more research to assess the perceptual threshold of direction-dependent characteristics in a decaying sound field [19, 20]. In [21], a perceptual study confirmed that spatial features of the late reverberation contribute to the feeling of envelopment of a listener. However, before a formal perceptual evaluation can be conducted, there is a need for new analysis methods suitable to assess objectively the characteristics of a decaying sound field [22–24].

Towards this goal, this paper proposes an analysis method capable of extracting direction-dependent characteristics within a captured SIR. Based on an existing analysis method, the Energy Decay Curves (EDC) [25], the proposed method consists of calculating the EDC for a set of Directional Impulse Responses (DIRs) [26] and comparing those results with with respect to a mean EDC, calculated from all directions, to obtain the Energy Decay Deviation (EDD). Through this method, the EDD can highlight the anisotropic features of a SIR and as such, is capable of quantifying the direction-dependent characteristics in a decaying sound field, which is an essential step in understanding how these characteristics are perceived by a listener.

Section 2 will cover background information relevant to the proposed method. Section 3 will introduce the EDD method along with possible design choices. In section 4, we will discuss three distinct results obtained with the proposed method. Finally, in the last section, we will discuss future work, research directions and conclude the paper.

2. BACKGROUND

2.1 Energy Decay Curve

The EDC was first introduced as a way to calculate the decay time within a noisy impulse response (IR) [25]. One of the goals of the EDC was to establish the decay time T_{60}. It was later expanded to the time-frequency domain through the Energy Decay Relief (EDR) [27]. The EDC consists of the reverse energy integration from an IR $h(t)$ which can be calculated at a time t with

$$\mathrm{EDC}(t) = \int_t^\infty h^2(\tau)\,\mathrm{d}\tau. \tag{1}$$

2.2 Mixing time

With the mixing time (t_{mix}), we aim to identify the moment where the reverberation transitions from early reflections to diffused late reverberation [6]. For SIRs, the measure of the sound field's diffuseness at different time segments can be used to determine the mixing time. For this purpose, an SIR diffuseness profile was calculated using the spatial covariance method [14] and averaged over the optimal frequency range for a given spherical microphone array. Diffuseness generally begins with low values, due to specular early reflections, and rapidly increases before reaching a relatively stable maximum value (Fig. 1). One way to define t_{mix} is as the moment a stable maximum is reached, and the diffuseness profile shows no more interference from discrete reflections, provided that the maximum is sufficiently high to be considered diffuse (e.g. ≥ 0.9) [28]. Thus the mixing time is calculated as

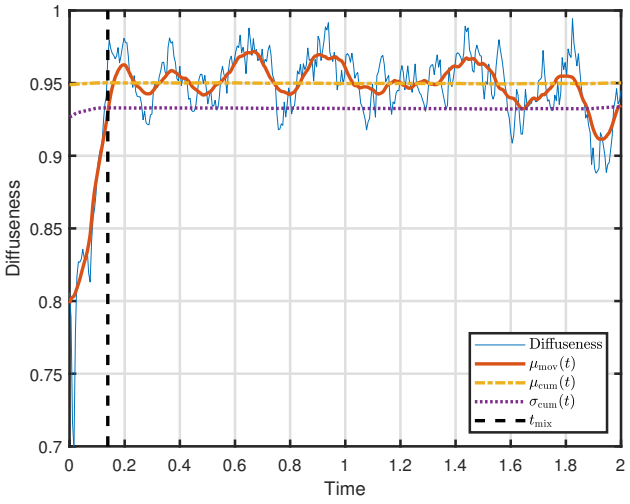

Figure 1. Example mixing time calculation using an SIR captured at the Church of Saint-Eustache in Paris, France, detailed in the results section

$$t_{\mathrm{mix}} = \min(t_d), \tag{2}$$

where t_d are the time values that satisfy the condition

$$\sqrt{\left[\mu_{\mathrm{mov}}(t_d) - \mu_{\mathrm{cum}}(t_d)\right]^2} \leq \sigma_{\mathrm{cum}}(t_d), \tag{3}$$

μ_{mov} is an appropriately-sized moving average of the diffuseness profile, μ_{cum} is its reverse-cumulative average, and σ_{cum} its reverse-cumulative standard deviation.

2.3 Noise floor time

One of the main weaknesses of the EDC integration is the contribution from non-decaying background noise present in a measured IR. Indeed, if the IR contains a long period of noise energy, it can have a significant impact on the EDC calculation and hide some details of the actual energy decay [29]. Several approaches exist to alleviate some of the adverse effects of background noise on the EDC calculation [30–32]. One simple approach is to crop the IR at time t_{noise} where the noise floor starts becoming noticeable in the response.

One method to identify t_{noise} is to first calculate the EDC of the omnidirectional channel of the SIR, then convert it to dB scale and segment the results using an adaptive

doi:10.25836/sasp.2019.32

Ramer-Douglas-Peucker algorithm [28]. The reverse integration of a non-decaying ideal dB-scale noise profile is then fitted by finding the best-matching segment. Finally, t_{noise} is defined as the last point above a specified headroom.

2.4 Beamforming

From the spherical harmonic decomposition of a sound field, we can extract the signals coming from specific incident directions using beamforming methods to obtain directional impulse responses (DIRs). The choice of a beamformer requires a compromise between the main lobe width and its amplitude or energy ratio with respect to the secondary lobes. For a spherical harmonic signal $\mathbf{s}$ at a given discrete time t, the signal y from an incident azimuth ϕ and elevation θ is given by

$$y(t, \phi, \theta) = \mathbf{w}_{\mathrm{PWD}}^{H}\, \mathbf{s}(t), \tag{4}$$

where $\mathbf{w}_{\mathrm{PWD}}$ contains the beamforming weights for the plane wave decomposition (PWD), obtained from

$$\mathbf{w}_{\mathrm{PWD}} = \mathbf{y}(\phi, \theta) \odot \mathbf{d}, \tag{5}$$

which represents the Hadamard product $\odot$ between $\mathbf{y}(\phi, \theta)$, the spherical harmonics vector for a given direction, and a weight vector $\mathbf{d}$ that can be used to change the shape of the beamformer [33, 34].

3. ENERGY DECAY DEVIATION

The main purpose of the EDD is to show the direction-dependent anisotropic characteristics throughout the decay by analyzing the per sample deviations to a mean EDC taken from every direction. Starting from an SIR, the first step is to extract the necessary DIRs for a chosen set of incident directions. From these DIRs, we can then calculate the directional EDCs, mean EDC, and directional EDDs. For analysis purposes, we are interested in a subset of directions that can have a meaningful representation. For instance, we can analyze the lateral plane by fixing the elevation θ to 0 and sampling the azimuth ϕ at fixed intervals.

Using a beamformer, we extract the directional signals from the SIR. As previously mentioned, it is important to bear in mind the shape of the beamformer's lobes when interpreting the results. The width of the main lobe will have a smoothing effect over multiple directions and thus, will reduce the dynamic range of the extracted signals. For the EDD, we chose an hypercardioid type of beamforming for its simplicity and the fact that it can extract signals with a maximum directivity index [33]. For this type of beamforming, the individual values of the $\mathbf{d}$ vector from Eq. 5 are all ones and therefore, the formulation can be simplified to

$$y(t, \phi, \theta) = \mathbf{y}(\phi, \theta)\, \mathbf{s}(t). \tag{6}$$

To prevent the adverse effect of the background noise detailed in Sec.2.3, the DIRs are cropped at time t_{noise}. An alternative method would be to replace the noisy parts of the signal, after t_{noise}, with an artificial noise signal which follows a predicted decaying curve [28].

The early part of the EDD tends to have the larger deviation due to the sparse early reflections. Although the EDD method is capable of showing the direction-dependent contribution of these early-reflections, we recommend cropping the beginning of the EDC before the t_{mix} time. By doing so, we can lower the necessary dynamic range of values used in the analysis of the remaining part of the EDD, which generally contains smaller EDD values. Other well-suited methods exist to analyze the precise direction of arrival (DOA) of early reflections [35]. For the same purpose, we also omit the last few samples of the EDD from the final analysis due to the statistical instability that occurs in very short integration times.

Therefore, we perform the EDC calculations of the extracted DIRs between t_{mix} and t_{noise} through the following reverse integration

$$\mathrm{EDC}(t, \phi, \theta) = \int_{t}^{t_{\mathrm{noise}}} y^2(\tau, \phi, \theta)\, \mathrm{d}\tau, \tag{7}$$

where $t > t_{\mathrm{mix}}$. We then convert these energy curves to the dB scale to perform the analysis on a scale closer to human auditory perception

$$\mathrm{EDC}_{\mathrm{dB}}(t, \phi, \theta) = 10\, \log_{10}(\mathrm{EDC}(t, \phi, \theta)). \tag{8}$$

Calculating the deviation of the EDC in the dB scale is one of the key difference between the proposed method and the method presented earlier in [26], where the same calculations are performed in the linear scale.

The next step to obtain the EDD is to calculate a reference mean $\overline{\mathrm{EDC}}_{\mathrm{dB}}$ for the chosen set of directions. The mean represents an ideal isotropic sound field

$$\overline{\mathrm{EDC}}_{\mathrm{dB}}(t) = \frac{1}{N} \sum_{i=0}^{N} \mathrm{EDC}_{dB}(t, \phi_i, \theta_i). \tag{9}$$

The final EDD is calculated for every directions from the deviation to that mean

$$\mathrm{EDD}(t, \phi, \theta) = \mathrm{EDC}_{\mathrm{dB}}(t, \phi, \theta) - \overline{\mathrm{EDC}}_{\mathrm{dB}}(t). \tag{10}$$

The EDD values represent how much energy remains in the decay when compared to $\overline{\mathrm{EDC}}_{\mathrm{dB}}$. The range of the deviation itself is also an important information in the EDD. Keeping in mind the smoothing caused by the beamformer, it can show narrow deviations which may still be perceived as isotropic. For frequency-dependent analysis, the input signals can be converted to the time-frequency domain before performing the above equations.

4. RESULTS

4.1 Simulated spatial impulse response

To validate the method, an artificial reference signal was generated with controlled direction-dependent characteristics. To construct the signal, we set a target direction-dependant decay time $T_{60}(\phi, \theta)$ for a set of uniformly distributed points around a sphere. We use a shape similar to a

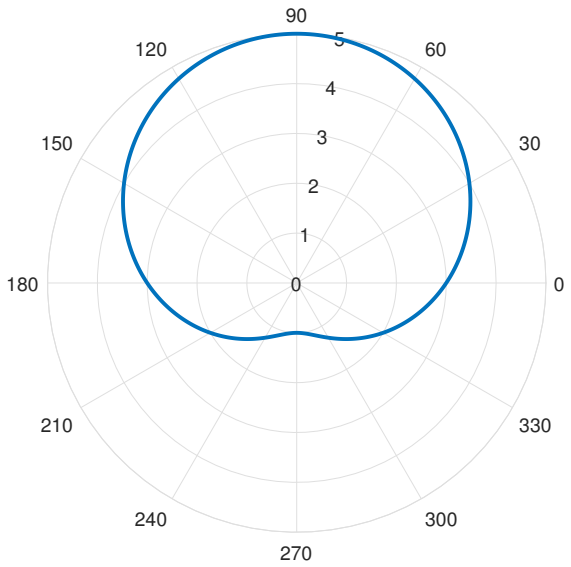

Figure 2. $T_{60}(\phi, 0°)$ of the artificial reference signal to show the distribution on the lateral plane.

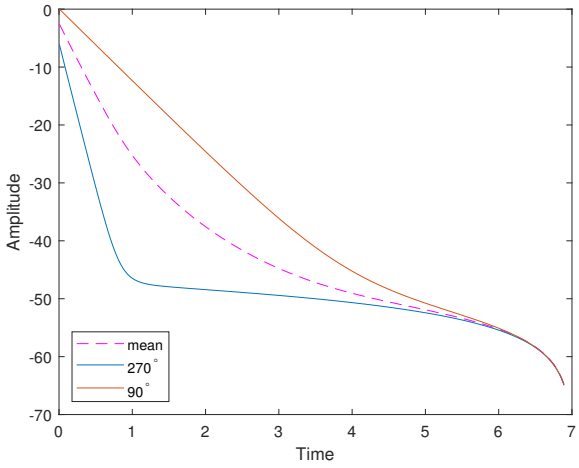

Figure 3. The $\overline{\mathrm{EDC}}_{\mathrm{dB}}$ of the simulated reference signal and the $\mathrm{EDC}_{\mathrm{dB}}(\phi, 0°)$ at $\phi = 90°$ and $\phi = 270°$.

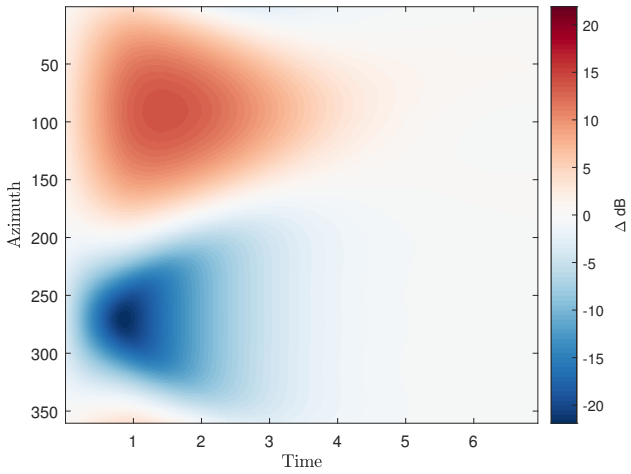

Figure 4. EDD of the reference signal, on the lateral plane.

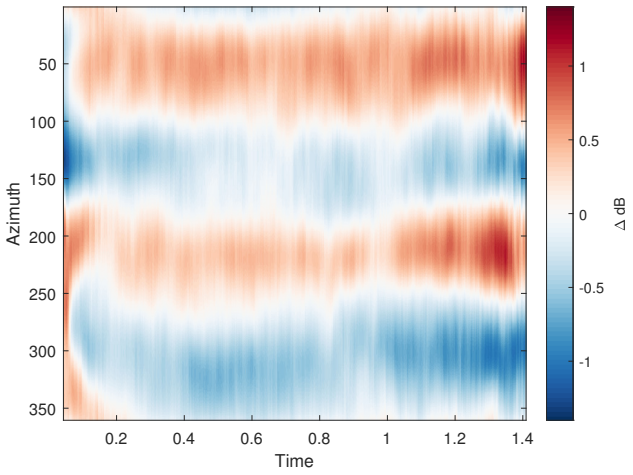

Figure 5. EDD of a long corridor with $t_{\mathrm{mix}} = 42.67$ milliseconds and $t_{\mathrm{noise}} = 1.456$ seconds. The minimum deviation is -1.34 dB and the maximum is 1.21 dB.

cardioid microphone pattern to distribute the $T_{60}(\phi, \theta)$ and create a recognizable shape in the decay (Fig. 2).

For each sampled point (ϕ_i, θ_i), we create an exponentially decaying Gaussian white noise signal that decays at the target rate $T_{60}(\phi_i, \theta_i)$. This signal is then mixed with another noise sequence with an amplitude set to -60 dB which represents the noise floor. These summed noise sequences are then encoded into fourth order ambisonics for each angle pair (ϕ_i, θ_i). The generated SIR signal is then analyzed using the EDD method. In Fig. 3 we can see how two specific $\mathrm{EDC}_{dB}(\phi_i, \theta_i)$ relate to the $\overline{\mathrm{EDC}}_{\mathrm{dB}}$ of the artificial signal. In Fig. 4, we can see the resulting EDDs on the horizontal plane. The red color show points where more energy remains in the decay, therefore showing directions with longer T_{60}, while the blue shows the opposite. The white color represents areas that follows the average. For illustration purposes, since the SIR was generated in controlled settings, the full signal was kept and not cropped as suggested in the method.

4.2 Measurement in a corridor

Next we look at the EDD of a long corridor that is 22 meters long, 2.8 meters wide and 3.2 meters tall. This SIR was recorded with a 32-channel spherical microphone array (Eigenmike®) at fourth order Ambisonics. This corridor is located on the campus of Aalto University in Espoo, Finland. The reverberation was first observed subjectively in that location to have a noticeably longer reverberation time in the direction of the long axis of the corridor. This can be confirmed with the EDD analysis of a captured SIR (Fig. 5). For the capture, the microphone was placed in the center of the room and the loudspeaker was placed 1.5 meters away from the microphone, between the wall and the microphone. In the EDD, we can observe some of the remaining early reflections characteristics before going into a stable direction-dependent energy distribution for the remaining of the decay. The direction-dependent characteristics for this SIR are distributed across 2.55 dB of deviation.

doi:10.25836/sasp.2019.32

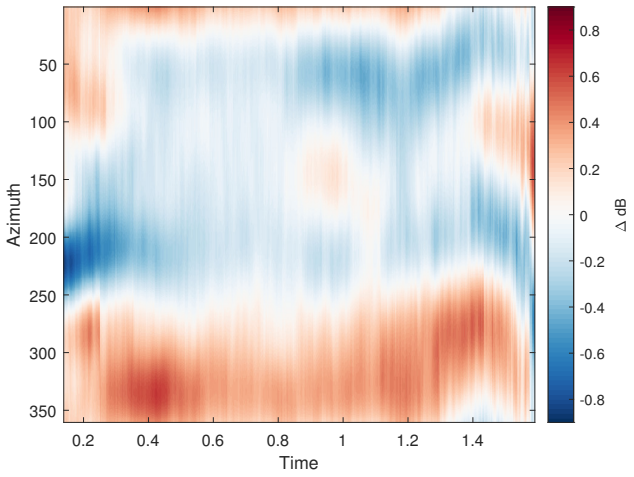

Figure 6. EDD of an SIR captured at the Saint-Eustache church. The $t_{\mathrm{mix}} = 138.67$ milliseconds and $t_{\mathrm{noise}} = 1.637$ seconds. The minimum deviation is -0.88 dB and the maximum is 0.64 dB.

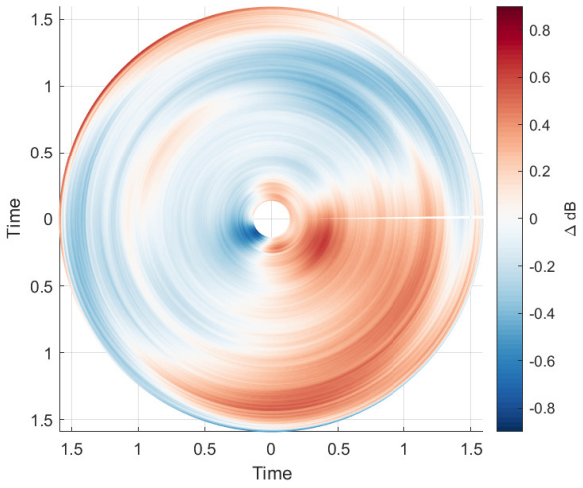

Figure 7. An alternate visualization of the EDD, using the data of Fig. 6, presented on the polar coordinate system to offer a more intuitive representation of directivity.

4.3 Measurement of the Church of Saint-Eustache

Finally, we calculated the EDD from a fourth order Ambisonics SIR captured at the Saint-Eustache church in Paris, France (Fig. 6). In this case, the direction-dependent characteristics are contained within a narrower range, 1.52 dB and it is not known at this point if they are perceptually noticeable. It is important here to reiterate the impact of the beamformer and note it is possible that the spatial smoothing hides larger deviations at narrower directions. Nonetheless, we were able to validate the stability of the EDD by comparing this result between multiple SIRs recorded from the same position (not shown due to space limitations).

We also propose an alternative representation, using a polar coordinate system, in which the radius represents time and the angles correspond to the incident direction of sound (Fig. 7). This form can show the characteristics more intuitively in applications where a lower resolution in the early decay is an acceptable compromise.

5. CONCLUSION

In conclusion, we introduced a formal method to analyze and assess the anisotropic features of an SIR. Based on the EDC, a popular analysis method for IRs, the proposed EDD measure can highlight direction-dependent characteristics in a decaying sound field. As such, it can serve as an analysis tool to study the behavior of late reverberation in more depth. This method benefits from using higher order ambisonics, to minimize the spatial smoothing caused by a beamformer. Future work includes analyzing different SIRs and conducting in depth perceptual studies to connect the directional characteristics of reverberation to the human auditory perception, as well as validating the use of denoising techniques to overcome the necessity of cropping the signal before the analysis.

6. ACKNOWLEDGEMENTS

Part of this work was conducted during Benoit Alary's research visit in October–December 2018, which was hosted by the UMR STMS (IRCAM-CNRS-Sorbonne Université) and was funded by the Foundation for Aalto University Science and Technology and by the Academy of Finland (ICHO project, Aalto University project no. 13296390).

7. REFERENCES

[1] A. D. Pierce, "Concept of a directional spectral energy density in room acoustics," *J. Acoust. Soc. Am.*, vol. 56, pp. 1304–1305, Oct. 1974.

[2] V. Välimäki, J. D. Parker, L. Savioja, J. O. Smith, and J. S. Abel, "Fifty years of artificial reverberation," *IEEE Trans. Audio Speech Lang. Process.*, vol. 20, pp. 1421–1448, Jul. 2012.

[3] M. R. Schroeder and B. F. Logan, "'Colorless' artificial reverberation," *J. Audio Eng. Soc.*, vol. 9, pp. 192–197, Jul. 1961.

[4] M. A. Gerzon, "Synthetic stereo reverberation, part I and II," *Studio Sound*, vol. 13(I), 14(II), pp. 632–635(I), 24–28(II), Dec. 1971(I), Jan. 1972(II).

[5] J. Stautner and M. Puckette, "Designing multi-channel reverberators," *Computer Music J.*, vol. 6, pp. 52–65, Spring 1982.

[6] J.-M. Jot, L. Cerveau, and O. Warusfel, "Analysis and synthesis of room reverberation based on a statistical time-frequency model," in *Proc. AES 103rd Conv.*, (New York, USA), Sep. 1997.

[7] B. A. Blesser, "An interdisciplinary synthesis of reverberation viewpoints," *J. Audio Eng. Soc*, vol. 49, pp. 867–903, Oct. 2001.

[8] S. Schlecht and E. Habets, "Feedback delay networks: Echo density and mixing time," *IEEE/ACM Trans. Audio Speech Lang. Process.*, vol. 25, pp. 374–383, Feb. 2017.

[9] V. Pulkki, "Spatial sound reproduction with directional audio coding," *J. Audio Eng. Soc.*, vol. 55, pp. 503–516, Jun. 2007.

[10] C. G. Balachandran and D. W. Robinson, "Diffusion of the decaying sound field," *Acta Acust.*, vol. 19, pp. 245–257, Jan. 1967.

[11] G. Bart, "Spatial cross-correlation in anisotropic sound fields," *Acta Acust.*, vol. 28, pp. 45–49, Jan. 1973.

[12] H. Cox, "Spatial correlation in arbitrary noise fields with application to ambient sea noise," *J. Acoust. Soc. Am.*, vol. 54, pp. 1289–1301, Nov. 1973.

[13] R. Talham, "Noise correlation functions for anisotropic noise fields," *J. Acoust. Soc. Am.*, vol. 69, pp. 213–215, Jan. 1981.

[14] N. Epain and C. T. Jin, "Spherical harmonic signal covariance and sound field diffuseness," *CoRR*, vol. abs/1607.00211, Jul. 2016.

[15] C.-H. Jeong, M. Nolan, and J. Balint, "Difficulties in comparing diffuse sound field measures and data/code sharing for future collaboration," in *Proc. Euronoise 2018*, (Heraklion, Crete), pp. 2005–2010, May 2018.

[16] J. Merimaa and V. Pulkki, "Spatial impulse response rendering I: Analysis and synthesis," *J. Audio Eng. Soc.*, vol. 53, pp. 1115–1127, Dec. 2005.

[17] S. Tervo, J. Ptynen, A. Kuusinen, and T. Lokki, "Spatial decomposition method for room impulse responses," *J. Audio Eng. Soc.*, vol. 61, pp. 17–28, Jan. 2013.

[18] B. Alary, A. Politis, S. J. Schlecht, and V. Välimäki, "Directional feedback delay network," *J. Audio Eng. Soc.*, in press 2019.

[19] D. Romblom, C. Guastavino, and P. Depalle, "Perceptual thresholds for non-ideal diffuse field reverberation," *J. Acoust. Soc. Am.*, vol. 140, pp. 3908–3916, Nov. 2016.

[20] P. Luizard, B. F. G. Katz, and C. Guastavino, "Perceptual thresholds for realistic double-slope decay reverberation in large coupled spaces," *J. Acoust. Soc. Am.*, vol. 137, pp. 75–84, Jan. 2015.

[21] W. Lachenmayr, A. Haapaniemi, and T. Lokki, "Direction of late reverberation and envelopment in two reproduced Berlin concert halls," in *Proc. AES 140th Conv.*, (Paris, France), Jun. 2016.

[22] M. Nolan, E. Fernandez-Grande, J. Brunskog, and C.-H. Jeong, "A wavenumber approach to quantifying the isotropy of the sound field in reverberant spaces," *J. Acoust. Soc. Am.*, vol. 143, pp. 2514–2526, Apr. 2018.

[23] T. Sakuma and K. Eda, "Energy decay analysis of non-diffuse sound fields in rectangular rooms," *Proc. of Meetings on Acoustics*, vol. 19, p. 015138, Jun. 2013.

[24] S. Oksanen, J. Parker, A. Politis, and V. Välimäki, "A directional diffuse reverberation model for excavated tunnels in rock," in *Proc. IEEE ICASSP-13*, (Vancouver, Canada), pp. 644–648, May 2013.

[25] M. R. Schroeder, "New method of measuring reverberation time," *J. Acoust. Soc. Am.*, vol. 37, pp. 409–412, Mar. 1965.

[26] M. Berzborn and M. Vorländer, "Investigations on the directional energy decay curves in reverberation rooms," in *Proc. Euronoise 2018*, (Heraklion, Crete, Greece), pp. 2005–2010, May 2018.

[27] J.-M. Jot, "An analysis/synthesis approach to real-time artificial reverberation," in *Proc. IEEE ICASSP-92*, vol. 2, (San Francisco, CA), pp. 221–224, Mar. 1992.

[28] P. Massé, T. Carpentier, O. Warusfel, and M. Noisternig, "Refinement and implementation of a robust directional room impulse response denoising process, including applications to highly varied measurement databases," in *Proc. ICSV26*, (Montréal, Canada), Jul. 2019.

[29] M. Karjalainen, P. Antsalo, A. Mäkivirta, T. Peltonen, and V. Välimäki, "Estimation of modal decay parameters from noisy response measurements," *J. Audio Eng. Soc.*, vol. 50, pp. 867–878, Nov. 2002.

[30] D. R. Morgan, "A parametric error analysis of the backward integration method for reverberation time estimation," *J. Acoust. Soc. Am.*, vol. 101, pp. 2686–2693, May 1997.

[31] L. Faiget, C. Legros, and R. Ruiz, "Optimization of the impulse response length: Application to noisy and highly reverberant rooms," *J. Audio Eng. Soc.*, vol. 46, pp. 741–750, Sep. 1998.

[32] Y. Hirata, "A method of eliminating noise in power responses," *J. Sound Vibr.*, vol. 82, pp. 593–595, Jun. 1982.

[33] B. Rafaely, *Fundamentals of Spherical Array Processing*. Springer, 2015.

[34] L. McCormack, S. Delikaris-Manias, and V. Pulkki, "Parametric acoustic camera for real-time sound capture, analysis and tracking," in *Proc. DAFx-17*, (Edinburgh, UK), pp. 412–419, Sep. 2017.

[35] S. Tervo and A. Politis, "Direction of arrival estimation of reflections from room impulse responses using a spherical microphone array," *IEEE/ACM Trans. Audio Speech Lang. Process.*, vol. 23, pp. 1539–1551, Oct. 2015.

 doi:10.25836/sasp.2019.32